Statistical Inference of Sound Speed and Attenuation Dispersion of a Fine-Grained Marine Sediment

David Paul Knobles ⬤, Christian D. Escobar-Amado, Michael J. Buckingham,
William S. Hodgkiss, *Life Member, IEEE*, Preston S. Wilson ⬤, Tracianne B. Neilsen, *Member, IEEE*,
Jie Yang ⬤, and Mohsen Badiey

Abstract—Acoustic recordings of signals in the 1.5–4.0-kHz band were analyzed for information about the sound speed and attenuation frequency dispersion of a fine-grained sediment found in the New England Mudpatch. Analysis of piston cores established prior bounds for a geophysical parameterization of a seabed model that predicts Kramers–Kronig dispersion relations. Sediment layers are described by the Buckingham viscous grain shearing (VGS) model that accounts for the effects of overburden pressure of compressional and shear speeds and attenuations. A statistical inverse problem was solved by using multiple samples of received levels recorded on two vertical line arrays as a function time and hydrophone depth for six frequencies in the 1.5–4.0-kHz band. A statistical inference model that assumed both model parameters and data samples are random variables quantified information content from marginalization of a conditional posterior probability distribution for the geophysical parameters that characterize the mud layer. From the inferred geophysical parameter point estimates the sediment sound speed and attenuation frequency dispersion are predicted and compared to previously reported direct measurements. Also, the predicted sound-speed gradient in the mud sediment from the VGS model is compared to a previous inference that utilized explosive sources.

Index Terms—Data ensemble maximum entropy (DEME), frequency dispersion, seabed geophysical parameters.

I. INTRODUCTION

AN IMPORTANT acoustic characteristic of a marine sediment is its frequency dependence or dispersion of the sound speed and attenuation. A goal for the Seabed Characterization Experiment 2017 was to use a combination of direct and acoustic measurements to infer the dispersion characteristics of a fine-grained sediment in the New England Mudpatch [1].

A fundamental question in remote sensing for ocean seabed characterization, such as frequency dispersion of sound speed and attenuation, is what additional information about the physical properties of the seabed not previously known or assumed known is gained from new measurments on an array of hydrophones or vector sensors. How does model complexity affect information content quantified by a conditional posterior probability distribution? Such information content can be degraded with increasing model complexity due to parameter correlations that leads to increased uncertainty [2].

This article focuses on the remote sensing of the geophysical properties of the upper portions (5 m) of a sediment composed of fine-grained materials generally possessing rigidity on the New England shelf studied by Twichell [3], Goff [4], and Chaytor [5]. Statistical inference techniques are applied to midfrequency acoustic data taken during the Seabed Characterization Experiment in 2017 to extract statistical properties of geophysical characteristics of the mud sediment from which the frequency dispersion of the sound speed and attenuation can be predicted [6]–[8]. From a Bayesian perspective, the piston core (PC) measurements made by Chaytor [5] act as *prior* information.

A complicating feature of this work is that a sediment generally has frequency dependent depth gradients of compressional and shear sound speeds and attenuations. Neglecting such gradients can bias estimates of the porosity and other parameters that are correlated with parameters such as sound speed and attenuation. The current analysis attempts to address this issue by using a new version of the viscous grain shearing (VGS) model [6]–[8] that accounts for the effects of overburden pressure through the depth effects of the compressional and shear modulus [9]. In this way, the gradients in the sound speed and attenuation are included implicitly as part of the model physics.

The rest of this article is organized as follows. Section II discusses the experimental measurements made during SBCEXP 2017. Section III discusses the geophysical model space. Section IV describes the analysis methodology that includes both a frequentist inference and a data ensemble maximum entropy (DEME) method. Section V presents the computational results and a discussion. Finally, Section VI concludes this article.

David Paul Knobles is with Knobles Scientific and Analysis, Austin, TX 78755 USA (e-mail: dpknobles@kphysics.org).

Christian D. Escobar-Amado and Mohsen Badiey are with the University of Delaware Newark, Newark, DE 19716 USA (e-mail: christiandavide@gmail.com; badiey@udel.edu).

Michael J. Buckingham is with the Scripps Institution of Oceanography, University of California, San Diego, La Jolla, CA 92093 USA (e-mail: mjb@mpl.ucsd.edu).

William S. Hodgkiss is with the Marine Physical Laboratory, Scripps Institution of Oceanography, University of California, San Diego, La Jolla, CA 92093 USA (e-mail: whodgkiss@ucsd.edu).

Preston S. Wilson is with the Mechanical Engineering Department and Applied Research Laboratories, University of Texas, Austin, TX 78713 USA (e-mail: pswilson@mail.utexas.edu).

Tracianne B. Neilsen is with Brigham Young University, Provo, UT 84602 USA (e-mail: tbn@byu.edu).

Jie Yang is with the Applied Physics Laboratory, University of Washington Seattle, Seattle, WA 98105 USA (e-mail: jieyang@apl.washington.edu).

Digital Object Identifier 10.1109/JOE.2021.3091846
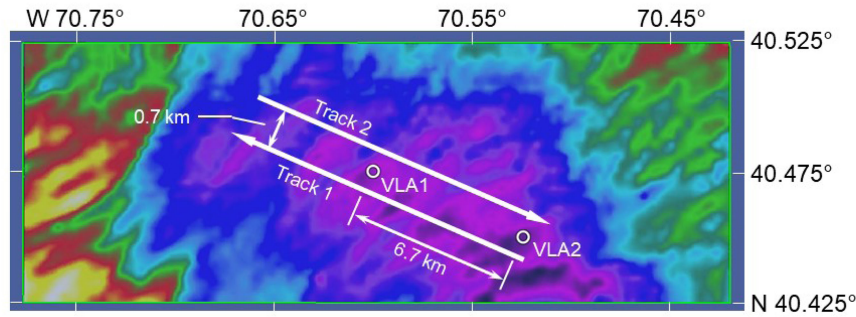
Fig. 1.   *RV Endeavor* tow tracks for ITC 2015 source and VLA locations. Data samples D_1, D_2, and D_3 were recorded as the towed source was moving along on Track 1, and D_4 and D_5 were recorded as the source was towed on Track 2.

II. EXPERIMENTAL DESIGN AND MEASUREMENTS

The acoustic measurements of interest in this article were made on March 24 (Day 083) 2017. Fig. 1 shows the experimental configuration where the *RV Endeavor* towed a ITC 2015 transducer emitting continuous wave sound radiation at discrete frequencies at approximately 1500, 2000, 2500, 3000, 3500, and 4000 Hz. Due to the Doppler effect the center frequencies for the six tonals differ by about 5–7 Hz depending on whether the source was moving toward or away from a receiver. The source tow experiment was made along a rectangular path with the two VLA arrays placed within the rectangle. The source tracks were positioned such that they were aligned with an NW to SE orientation of the central channel of mud that defines the Mudpatch [4]. The nominal tow depth and speed were about 45 m and 3 kn, respectively. The geographical position of the Scripps Marine Physics Laboratory VLA 1 and VLA 2 were about 40 28.207° N 70 35.8266° W and 40 26.5073° N 70 31.6299° W, respectively. The two VLAs were approximately identical in that the bottom phone of each array was located at about 5 m above the water-seabed interface with a constant hydrophone spacing of 3.75 m, giving a total vertical aperture of 60 m. The water depth at both arrays was about 74.5 m.

The notation D_1 in Fig. 1 corresponds to a data sample recorded on VLA 2 over a time interval when the source was on Track 1 and moved in an NW direction away from VLA 2. Also, D_1 is a rectangular matrix of received levels, in dB rel 1μPa, where the rows refer to a relative time with spacing of 0.5 s and the columns refer to hydrophone channel and frequency. There are 16 hydrophones that span 60 m of the water column. The data samples are all processed such that the first time sample corresponds to the source being at the closest point of approach (CPA) on the track. For sources approaching an array, this means that the data component in time was *flipped*. For each hydrophone/channel, the levels are included at six frequencies with channel 1 in the first column, followed by channel 2, etc., for a total number of $16 \times 6 = 96$ columns. The number of row elements is 8850. At 3 kn (1.543 m/s) each data sample corresponds to the source moving a total distance of about 6800 m. D_2 and D_3 refer to data samples recorded on VLA 1 where the source moved toward and away from the array on Track 1, respectively. D_4 and D_5 refer to data samples recorded on VLA 1 where the source moved toward and away
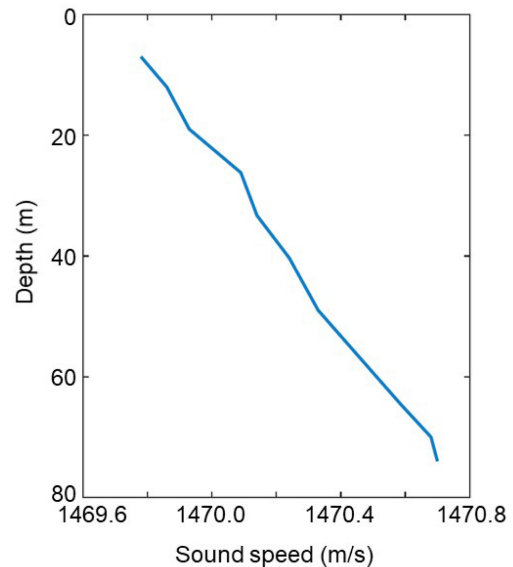

Fig. 2.   SSP derived from CTD cast 03 from *RV Endeavor* on Julian day 82 hour 19, minute 12.

from the array on Track 2, respectively. D_6 refers to data samples recorded on VLA 2 where the source moved toward the array on Track 2. Analysis of the D_6 data sample, however, is beyond the scope of this article due to an inability reconcile certain signal processing criteria that apparently were a result of nonuniform motion of the source near the array. Such time periods occurred during the experiments due to the need to avoid fishing gear that was present in the area in large quantities.

Fig. 2 shows a sound-speed profile (SSP) derived from CTD measurements made on *RV Endeavor* on the day that the mid-frequency acoustic data were collected. Over the course of this five-day period, warmer water slowly entered into the experimental area over the full volume of the water column causing the sound speed to slowly increase uniformly with depth. However, the sound-speed gradient was stable, about $+0.016$ 1/s. In all the computations presented in this study, the SSP was assumed fixed and was the profile that was measured closest in time to the acoustic measurements. In general, the benign properties of the water column offered a rare opportunity to apply a matched-field

inversion method where the errors were dominated by seabed model mismatch as opposed to mismatch with the SSP.

A challenging aspect of the analysis was that because of marine mammal environmental regulations the duty cycle of the source was 50%, specifically 10 s on and 10 s off. To mitigate the effects of the duty cycle on the inference of information content, the data underwent a signal processing method where the peak envelopes of the received levels were extracted followed by a spline fit to the peak values. Specifically, the MATLAB function $[\mathrm{yupper}, \mathrm{ylower}] = \mathrm{envelope}\,(x, np, \text{"peak"})$ was utilized where yupper was chosen to return the upper envelopes of data x determined using spline interpolation over local maxima separated by at least np samples. By *trial and error* an optimal value of np was estimated to be about 30 for the VLA data set. The idea was to prevent a matched-field-based inversion approach from *mistaking* off-times of the source with nulls in the acoustic field that result from modal destructive interference. To be consistent, each modeled acoustic field hypothesis also underwent the same envelope processing in the evaluation of the error function [see (18)]. It was necessary to eliminate points near the start and end data and model time samples to account for the fact that spline fitting can give spuriously large values near the end points. Instead of fitting the finer details of modal interference patterns, the emphasis is the envelope structure of the field. The price to pay for stability and consistency for both model and data are a certain loss of information. It will be seen that important information gain about critical geophysical parameters can still be obtained if the sediment model chosen has an adequate balance of simplicity and physical constraints.

III. PROPOSED GEOPHYSICAL, SOURCE MOTION, AND PROPAGATION MODELS

This work considers a seabed model based on the VGS theory where each layer is characterized by N, ρ_0, ρ_g, K_0, k_g, μ_g, n, τ, and c_0, which symbolize the porosity, the wet bulk density, the grain density, the wet bulk modulus, the grain bulk modulus, the grain size, the shear hardening index, the viscous time constant, and the Wood–Mallock sound speed, respectively. The viscous time constant τ, and the strain hardening index n provide an empirical description of an effective grain-to-grain contact in the acoustic response of the sediment. Each sediment layer has its own dispersion characteristics of compressional and shear sound speed and attenuation. In addition, each layer has a depth dependence of compressional and shear speeds and attenuations and is described in [9]. The low-frequency limit of the VGS model is the sediment suspension theory described by the Wood–Mallock equations [10] and [11], with K_w and ρ_w as the bulk modulus and density of the water

$$c_0 = \sqrt{\frac{K_0}{\rho_0}} \qquad (1)$$

where

$$\frac{1}{(K_0)} = \frac{N}{(K_w)} + \frac{(1 - N)}{(K_g)} \qquad (2)$$

and

$$\rho_0(N) = \rho_g + N(\rho_w - \rho_g). \qquad (3)$$

Chaytor [5] reports that for the New England Mudpatch, the grain density of the mud is $< \rho_g > = 2500$ kg/m^3, which is consistent with the value of 2499 kg/m^3 inferred in [12] that employed SUS explosive charges to estimate a low-frequency geoacoustic profile for the Mudpatch. Assuming a value for ρ_w of 1030 kg/m^3, (3) provides a linear relationship for $\rho_0(N)$. Following Buckingham [8], an expression for grain size is

$$\mu_g(N) = \frac{2\Delta(2B - 1)}{1 - B} \qquad (4)$$

where

$$B = \left(\frac{1 - N}{1 - N_{\min}}\right)^{1/3} \qquad (5)$$

with $N_{\min} = 0.37$. The roughness parameter is defined as $\Delta = 1\ \mu\mathrm{m}$ [13]. In units of Krumbein ϕ scale [14], the grain size can be expressed as

$$\phi = -\log_2(\mu_g/\mu_0) \qquad (6)$$

where $\mu_0 = 1000\ \mu\mathrm{m}$.

The basic geophysical parameters for the mud sediment and the deeper layers are shown in Table I. Parameter values are either fixed or have upper and lower bounds that define a search space. Between the upper and lower bounds, it is assumed that the prior probability distribution is uniform. Chaytor's analysis [5] suggests that the upper portion of the mud is a mixture of about 30% sand, 50% silt, and 20% clay. The sediment composition changes to 10%–20% sand, 60% silt, and 10% clay below about 2 m. Additional parameters include the compressional modulus, the shear modulus, the shear coefficient, and the grain shearing coefficient, all of which are held fixed based on the work by Buckingham [8] and Richardson [13]. The remainder of the layers are assumed fixed from previous results. Each layer has a depth dependence due to overburden pressure; this dependence is specified by the depth dependence of the compressional and shear modulus and is described in [9]. The resulting depth dependence for both the compressional and shear sound speeds and attenuations generally vary with frequency and nonlinearly with depth. At every depth, the compressional speed and attenuation satisfy a Kramers–Kronig dispersion relationship [15]–[17].

The VGS theory was originally derived in connection with coarser sediments, the sands and silts, in which the grains are roughly spherical in shape. It has been found, however that the VGS dispersion relations provide a reasonable representation of the wave speeds and attenuations, not only in sands but also in the finer-grained materials, such as the clays and muds. Many of the mineral particles found in mud are far from spherical, taking the form of high-aspect-ratio needles or platelets, which raises the question as to why VGS matches the fine-grain dispersion data so well? It has been argued in [9] that the geometrical shapes of the particles are immaterial, the important factor in VGS being the detailed nature of the contact between one particle and another. In the context of such a contact, the point of a needle is much the same as a sphere with the same radius of curvature. More details are given in [9], but the essential conclusion, which is supported by experimental evidence, is that the VGS theory has application to compressional waves and shear waves in a wide range of

TABLE I
GEOPHYSICAL PARAMETERS FOR MULTILAYERED REPRESENTATION OF SEABED

Parameter, symbol,	Mud	T_1	T_2	T_3	S	units
Content, –	clayey silt	sand-silt-clay	sand-silt-clay	sand-silt-clay	fine to medium sand	–
Layer thickness, LT	9.3	1.0	1.0	1.0	5.0	m
Porosity, N	[0.563 –0.640]	0.563	0.52	0.50	0.40	——
Bulk density, ρ_0	Eq. 3	1645	1648	1700	1963	$\frac{kg}{m^3}$
Grain density, ρ_g	2500	Eq. 3	Eq. 3	Eq. 3	Eq. 3	$\frac{kg}{m^3}$
Mean grain diameter, μ_g	Eqs. 4-6	Eqs. 4-6	Eqs. 4-6	Eqs. 4-6	Eqs. 4-6	ϕ
Mineral grain bulk modulus, K_g	[13.5–15.5]	15	30	32	32	GPa
Sediment bulk modulus, K_0	Eq. 2	Eq. 2	Eq. 2	Eq. 2	Eq. 2	GPa
Woods Mallock sound speed, c_0	Eq. 1	Eq. 1	Eq. 1	Eq. 1	Eq. 1	m/s
Compressional modulus, γ_p	7.01E07	7.01E07	7.01E07	7.01E07	7.01E07	Pa
Shear modulus, γ_s	1.75E06	1.75E06	1.75E06	1.75E06	1.75E06	Pa
Strain hardening index, n	[0.01–0.1]	0.05	0.0384	0.08854	0.08854	——
Visco-elastic time constant, τ	∞	0.01	0.0012	0.00012	0.00012	s
Compressional coefficient, γ_{p0}	3.54E08	3.54E08	3.54E08	3.54E08	3.54E08	Pa
Shear coefficient, γ_{s0}	4.47E07	4.47E07	4.47E07	4.47E07	4.47E07	Pa
Grain shearing coefficient, Ξ	0.022	0.022	0.022	0.022	0.022	Pa

The parameters in bold face for the mud layer along with the speed of the source are those that form the hypothesis space.

sediments, from coarse sands to fine grained muds and clays, making it an appropriate choice for representing the stratified sediment at the New England Mudpatch.

Three parameters in the mud layer are viewed as unknown or random, and in Table I, the lower and upper parameter bounds are presented in brackets. The upper and lower bounds for N were provided by Chaytor [5]. The upper and lower bounds for n are based on values reported by Buckingham [8]. Buckhingham has noted that a significant amount of data can be explained by setting n to be 0.0866. Generally, smaller values of n are indicative of a softer sediment. Since the mud sediment is reportedly a mixture of clays, silts, and sands, n is allowed to vary between 0.01 and 0.10. The upper and lower bounds for the grain bulk modulus for the mud were reported by Chaytor [5]. The remainder parameters in the mud layer are assumed known. For example, it was decided to fix the value of τ to infinity because [1] suggested that to first order there was only a small degree of frequency dispersion of the sound-speed ratio (SSR) in the 100–100 000-Hz band. Most specifically, there does not appear strong evidence of a transition frequency that would be proportional to the inverse of τ. It is of interest to note that in the limit that τ goes to infinity, the VGS theory reduces to the original grain shearing model.

The sediment characterization of layers beneath the fixed mud layer are based on previous results. For example, Twichell [3], Goff [4], and Chaytor [5] report on the existence of a *transition layer* from the mud to the sand layer. The transition layer has been reported to have a thickness of 2–3 m. In this work, we fixed this layer thickness at 3 m, but made the layer have a more continuous transition by dividing it into three 1 m layers with decreasing porosity. Namely, a depth gradient of the physical parameters was introduced for the sediment to vary from mud to sand. The transition layer has also been inferred from the analyses of acoustic data (see, for example, [18] and [19]) using trans-dimensional Bayesian inversion processing. The assumed

properties of the sand layer are based mostly on finding porosity values that, when used in the VGS model would predict the reported sound speeds by Yang [20]. No attempt at inverting for parameters in these deeper layers was made because due to the lack of information content in the 1.5–4.0-kHz band and at the long ranges. In other words, the acoustic field that penetrated into the seabed in the 1.5–4.0-kHz band was for the most part confined to the first 5 m or so of the mud.

In the simple case of uniform source motion (assumed in this article), $\mathcal{X}_s(t)$ is represented by a straight line or track that has a closest position of approach (CPA) range (r_{cpa}) to a VLA. At any point on this track, the distance or range from the source to the receiver r is

$$r(t) = \sqrt{(r_{\mathrm{cpa}})^2 + (\mathcal{X}_s(t))^2} \qquad (7)$$

where

$$\mathcal{X}_s(t) = \mathcal{X}_s(t=0) + St \qquad (8)$$

and S is the speed of *RV Endeavor*. The reported source depth was 45 m and is held fixed. In this study, the CPA range is assumed fixed, but the speed is viewed as a random parameter with upper and lower bounds of 2.8 and 3.3 kn, respectively.

For each sampling of the hypothesis space, the frequency and depth-dependent sound speeds and attenuations computed with the VGS model along with source parameters are then input into a broadband elastic normal mode algorithm [21]. The resulting received pressure field $\mathcal{P}$ in cylindrical coordinates is then computed as

$$\mathcal{P}(f, z, r) = 10^{\mathrm{SL}/20} * \mathcal{G} \qquad (9)$$

where $\mathcal{G}$ is the complex Green's function solution to the Helmholtz equation for a unit point source

$$\mathcal{G}(f, z_s, z, r) = \frac{i}{4\rho(z_s)} \sum_m \phi_m(z_s)\phi_m(z)H_0^1(k_m r) \qquad (10)$$

where k_m and ϕ_m are the horizontal wave number eigenvalues and depth dependent eigenfunctions, respectively. $\mathrm{SL}(f)$ are the source levels and are assumed fixed from measurement (deterministic).

IV. STATISTICAL INFERENCE METHODS

The following two procedures of analyses are considered: a *frequentist* methodology and a DEME approach.

A. Frequentist Statistics

Frequentist statistics [22] are based on an estimate $\boldsymbol{\Theta}_{\mathrm{est}}$ of a vector of parameter values from multiple measurements, and then using this estimate when making all predictions of, for example, the received acoustic level $\mathrm{RL}(\boldsymbol{\Theta}_{\mathrm{est}})$. The notation used in this discussion is that $\boldsymbol{\Theta}$ is a vector with components $(\Theta_1, \Theta_2, \ldots \Theta_{K-1}, \Theta_K)$. Frequentists assume that the true value $\boldsymbol{\Theta}_{\mathrm{true}}$ is fixed (deterministic) but unknown, and that $\boldsymbol{\Theta}_{\mathrm{est}}$ is a *reasonable* approximation to $\boldsymbol{\Theta}_{\mathrm{true}}$. However, it is assumed that the data $(\mathbf{D}_1, \mathbf{D}_2, \ldots \mathbf{D}_{M-1}, \mathbf{D}_M)$ are not fixed, but are random. In the frequentist method, a point estimate is the single best parameter value estimate of $\hat{\boldsymbol{\Theta}}_{\mathrm{true}}$ found by minimizing an error function, $E(\boldsymbol{\Theta}, \mathbf{D}_m)$. Mathematically this idea is expressed as

$$\hat{\boldsymbol{\Theta}}_m = \mathrm{Argmin}_{\boldsymbol{\Theta}}\, E(\boldsymbol{\Theta}_m, \mathbf{D}_m), \quad m = 1, 2, \ldots, M. \quad (11)$$

This point estimate is a random variable because the data sample is a random selection from a probability distribution of samples. The main problem with such a point estimate based on a single data sample is that there is no uncertainty. However, multiple data sets do allow one to find an average and a standard deviation for each parameter, even though an individual result has no uncertainty. This is fully analogous to rolling dice.

B. Data and Environmental Ensemble Maximum Entropy Statistics

The DEME method as implemented by Knobles *et al.* [12], [23], [24] in remote sensing applications in ocean acoustics has its origins with the early works of Cox [2], Kullback [25], Jaynes [26]–[27], and Bilbro [28] that demonstrated the connectivity of machine learning and maximum entropy. A question that arises for DEME is how many data samples can be in the data resemble before the addition of a new sample gives no additional information other than the statistic. When the size of the data ensemble space reaches this size, one can say that statistical sufficiency has been reached. For a reference on information and sufficiency the reader is also referred to Jayne's classic book on probability theory [29].

Before making a comment on DEME, it is useful to point out the differences between frequentist and Bayesian concepts in probability theory. Instead of using only $\hat{\Theta}$ to make predictions, a Bayesian approach considers all possible values of $\boldsymbol{\Theta}$ to compute a probability distribution to ascertain the degree of certainty for various $\boldsymbol{\Theta}$ values. Also, in contrast to a frequentist approach the parameters in $\boldsymbol{\Theta}$ are nondeterministic and, thus, represented as random variables. Furthermore, in a Bayesian

method, the data are fixed, namely, the data are deterministic. The goal of the Bayesian model is to quantify questions about information content and sufficiency. For example, the Bayesian concept quantifies the information that the data contain that the prior information did not? It also addresses how much parameter correlations [2] contribute to the uncertainty for a given parameter.

To be consistent in the analysis of remote sensing data, both the data and the model parameters should be treated as nondeterministic. This is the essence of DEME [12], [23], [24] whose goal, such as a Bayesian method, is to construct a conditional posterior probability distribution $P(\boldsymbol{\Theta}_m|\mathbf{D}_m)$ for $m = 1, 2, \ldots M$ from which marginal probability distributions can be computed. One can then average the marginal distributions over the data samples to obtain a more realistic assessment of the uncertainty of the parameter inference. The conditional marginal distribution for the parameter θ_k and data sample $\mathbf{D}_m$ is

$$P_m(\theta_k|\mathbf{D}_m) = \int d\theta_1 d\theta_2 \cdots d\theta_{k-1} d\theta_{k+1} \cdots d\theta_M P(\boldsymbol{\Theta}|\mathbf{D_m}) \quad (12)$$

with

$$P(\theta_k|\mathbf{D}_m) = P(\theta_k)\frac{\exp[-\beta_m \mathcal{E}_m(\theta_k, \mathbf{D}_m)]}{Z_m} \quad (13)$$

where $\mathcal{E}_m$ is an error function. Z_m and β_m are analogous to the partition function and the Boltzmann factor, respectively, with

$$Z(\beta_m) = \int dH P(H)\exp[-\beta_m \mathcal{E}_m(\theta_k, \mathbf{D}_m)] \quad (14)$$

and where β_m is determined by solving a constraint integral equation.

From the marginals, we can, for example, find the expectation of θ from the distributions

$$E_m(\theta_k) = \int d\theta_k\, \theta_k P_m(\theta_k|\mathbf{D}_m). \quad (15)$$

One can also define an average marginal distribution

$$< P(\theta_k) >= \frac{1}{M}\sum_m P_m(\theta_k|\mathbf{D}_m) \quad (16)$$

from which

$$E(\theta_k) = \int d\theta_k\, \theta_k\, < P(\theta_k) > . \quad (17)$$

Finally, the error function utilized in the construction of the posterior distribution is a squared error

$$\mathcal{E}(\boldsymbol{\Theta}, \mathbf{D}) = \sum_{\mathbf{i}}\sum_{\mathbf{j}}\sum_{\mathbf{k}}(\mathbf{D}(\mathbf{f_i}, \mathbf{z_j}, \mathbf{r_k}) - \mathcal{D_s}(\mathbf{f_i}, \mathbf{z_j}, \mathbf{r_k}))^{\mathbf{2}} \quad (18)$$

where

$$\mathcal{D}_s = 20 \log_{10}|\mathcal{P}(f, z, r)| \quad (19)$$

where $\mathcal{P}(f, z, r)$ is given in (9) and (10) and f_i, z_j, r_k represent frequency, receiver depth, and source–receiver range (7).

TABLE II
$\hat{\theta}_j$ Found Via Monte Carlo Method With 200 000 Samples of Θ

Data sample	N	n	k_g (Pa)	S(knots)	$E(\hat{\theta}_n)$ (dB^2)
1	0.5959	0.0627	1.4442×10^{10}	3.341	1.42×10^7
2	0.5881	0.0611	1.4444×10^{10}	3.175	1.36×10^7
3	0.5763	0.0471	1.4479×10^{10}	3.197	1.47×10^7
4	0.6274	0.0599	1.3580×10^{10}	3.096	1.29×10^7
5	0.5817	0.0476	1.4852×10^{10}	3.241	1.48×10^7
mean	0.59388	0.05568	1.44×10^{10}	3.21	—
std	0.01799	0.00686	4.19×10^8	0.08	—

TABLE III
$E_m(\theta_k)$ for $m = 1, 2, \ldots, M$ and $E(\theta_k)$ and Standard Deviations

Data sample	N	n	k_g (Pa)	S (knots)
1	$0.6026 \pm .014$	$0.0658 \pm .012$	$1.4508 \times 10^{10} \pm 6.21698 \times 10^8$	3.2837 ± 0.1792
2	$0.5892 \pm .0153$	$0.0599 \pm .0182$	$1.4481 \times 10^{10} \pm 6.0823 \times 10^8$	3.1596 ± 0.1729
3	$0.5829 \pm .0119$	$0.0614 \pm .0213$	$1.4543 \times 10^{10} \pm 6.1 \times 10^8$	3.2619 ± 0.1338
4	$0.6086 \pm .0166$	$0.0684 \pm .0201$	$1.441 \times 10^{10} \pm 6.2778 \times 10^8$	3.2598 ± 0.133
5	$0.5826 \pm .012$	$0.05818 \pm .0201$	$1.4543 \times 10^{10} \pm 6.0108 \times 10^8$	3.2773 ± 0.1294
mean of $< P(\theta_k) >$	0.59318	0.064	1.45×10^{10}	3.28
std relative to mean	0.01058	0.003658	5.122×10^7	0.044

V. Scientific Findings

The five data samples from the midfrequency towed source recorded on the VLAs are used to estimate four parameters. The full parameter space consists of

$$\Theta = (N, n, k_g, S) \qquad (20)$$

where S is the speed of the source. The CPA ranges are held fixed at the measured value provided by global positioning measurements and are 364, 378, 378, 324, and 324 m for the collection of samples $\mathbf{D}_1, \mathbf{D}_2, \mathbf{D}_3, \mathbf{D}_4$, and $\mathbf{D}_5$, respectively.

The following four point estimates are computed to generate modeled transmission loss that can be compared to measured TL.

1) Optimal inversion solution $\hat{\Theta}_m, m = 1, 2, \ldots, M$.

2) Frequentist average of $\hat{\Theta}_m$ over data samples, via Monte Carlo sampling shown in Table II

$$< \Theta > = \frac{1}{\mathbf{M}} \sum_{\mathbf{m}} \hat{\Theta}_\mathbf{m}. \qquad (21)$$

3) Expectation of parameters from marginals $P_m(\theta_k | \mathbf{D}_m)$ for $m = 1, 2, \ldots, M$ (15) shown in Table III

$$E_m(\theta_k) = \int d\theta_k \, \theta_k P_m(\theta_k | \mathbf{D}_m). \qquad (22)$$

4) Expectation from ensemble averaged marginals (17) shown in Table III

$$E(\theta_k) = \int d\theta_k \, \theta_k \, < P(\theta_k) > . \qquad (23)$$

Table II shows the frequentist results for the point estimates that correspond to the optimized results for $\mathbf{D_m}; m = 1, \ldots, 5$. The optimal solutions $\hat{\Theta}_m$ were found with Monte Carlo sampling of the hypothesis space. It was generally found that 200 000 random samples of $\hat{\Theta}_m$ was sufficient in finding $\hat{\Theta}_m$. A problem with a frequentist prediction is that it cannot address the question of whether the number of data samples provided additional information mentioned above that provided by the priors.

Fig. 3 shows the marginal probability distributions $P_m(\theta_k | \mathbf{D}_m)$ $m = 1, 2, \ldots, 5$ using the DEME method. With the exception of $P_4(\theta_k | \mathbf{D}_4)$, the distributions for N, n, and S are single-peaked with a modicum degree of symmetry, while the distributions for k_g are essentially flat. Relative to the uniform prior distributions information was clearly gained for N, n, and S while essentially no information was gained for k_g. $P_4(\theta_k | \mathbf{D}_4)$ has distributions for N and n that have a non-Gaussian form. Fig. 3 also shows the distributions for the average distributions $< P(\theta_k) >$. The fact that the average marginal distributions are also generally peaked demonstrates that the standard deviations of the marginals are small and do not have a large off-set for different data sample m values. This is suggestive that for at least $P_m; j = 1, 2, 3, 5$ the data samples belong to the same statistical distribution, which in turn suggests that the mud variability in the area of the tow track rectangle in Fig. 1 is generally small.

Table III shows the statistic results for the point estimates that correspond to the average values from the marginal distributions. There is good agreement between the optimized results in Table II and the average results in Table III. However, an important point is that one would not have known if the point estimates
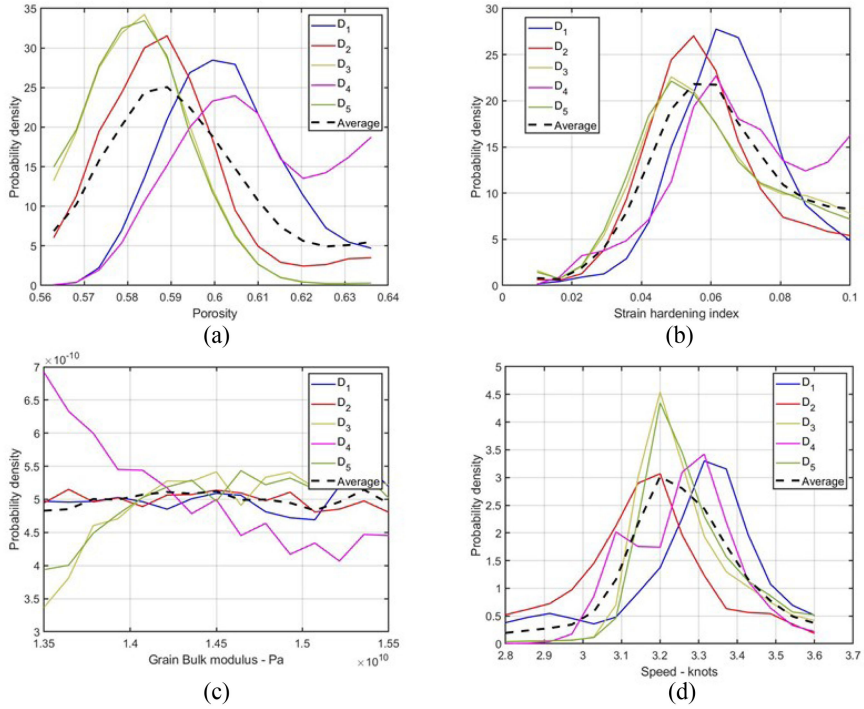
Fig. 3. Marginal distributions $P_m(\theta_k|D_m)$ for (a) N, (b) n, (c) k_g, and (d) S for $j = 1, 2, 3, 4,$ and 5 and average distributions.
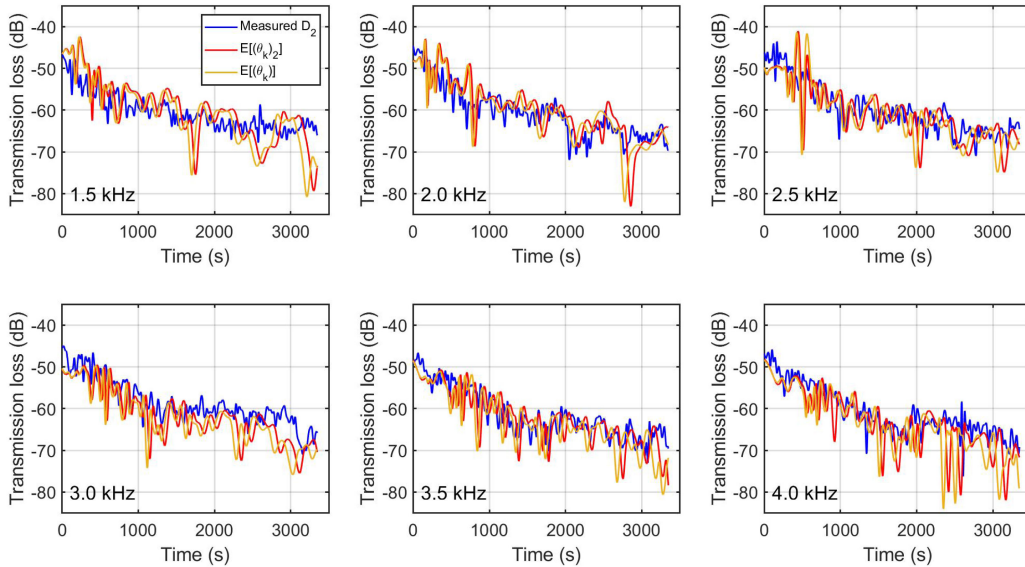

Fig. 4. Comparison of and measured TL for $\mathbf{D_2}$ on hydrophone 16 with modeled TL using parameter expectation values $E_2[(\theta_k)]$ and $E[\theta_k)]$.

that used the optimal results (see Table II) made sense unless the DEME computations that provided the estimates based on the marginal distributions in Fig. 3 had been made.

Fig. 4 shows the data-model comparisons for the transmission loss (TL = RL − SL) as a function of time for the six tonal frequencies using the $\mathbf{D_2}$ on hydrophone 16 with modeled TL using parameter expectation values $E_2[(\theta_k)]$ and $E[(\theta_k)]$. The difference in the two modeled solutions is small, and overall there is qualitative agreement between the modeled solutions and the measured TL.

Fig. 5 is the same as Fig. 4 except that the two modeled solutions are $E_4[(\theta_k)]$ and $E[(\theta_k)]$. There are larger difference between the modeled solutions $E_4[(\theta_k)]$ and $E[(\theta_k)]$. The larger differences may be ascribed to the previous observation in Fig. 3 that of the five data samples, the marginals produced had non-Gaussian attributes, and thus, $E_4[(\theta_k)]$ and $E[(\theta_k)]$ have larger differences.

Fig. 6 shows the predicted sediment depth-dependent compressional and shear sound speed and attenuation for the $E(\theta_k)$ VGS parameter values in Table III. For the compressional sound
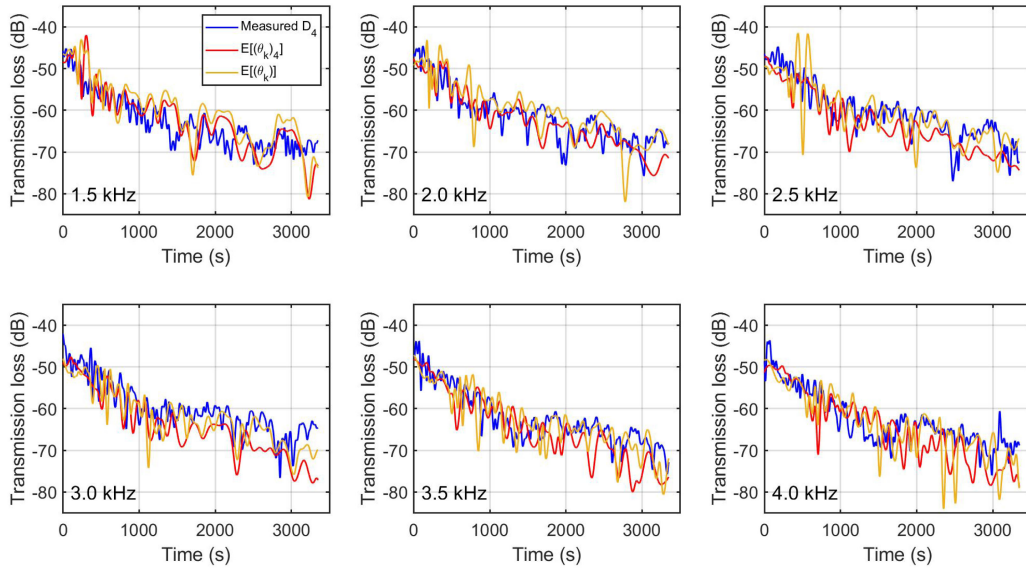
Fig. 5.   Comparison of and measured TL for $\mathbf{D_4}$ on hydrophone 16 with modeled TL using parameter expectation values $E_4[(\theta_k)]$ and $E[\theta_k)]$.
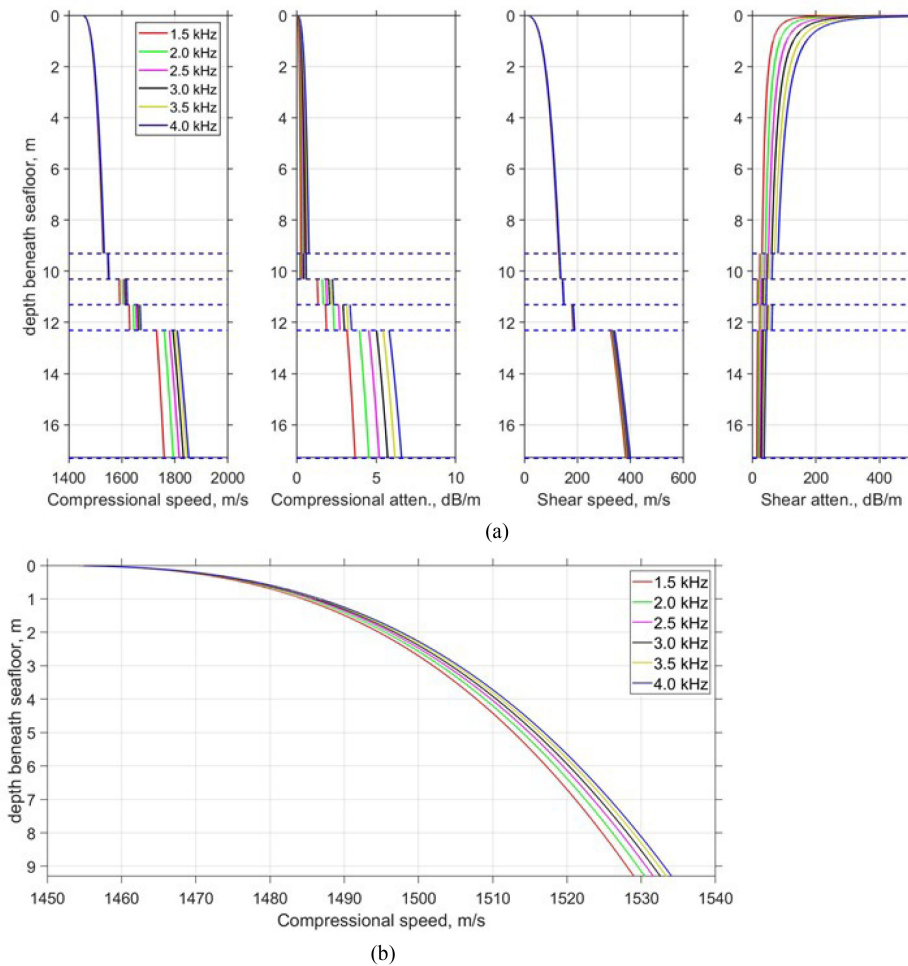

Fig. 6.   Predicted depth dependence of mud sediment parameters with VGS theory. (a) Compressional sound speed, compressional attenuation, shear sound speed, and shear attenuation. (b) High resolution of compressional sound speed.
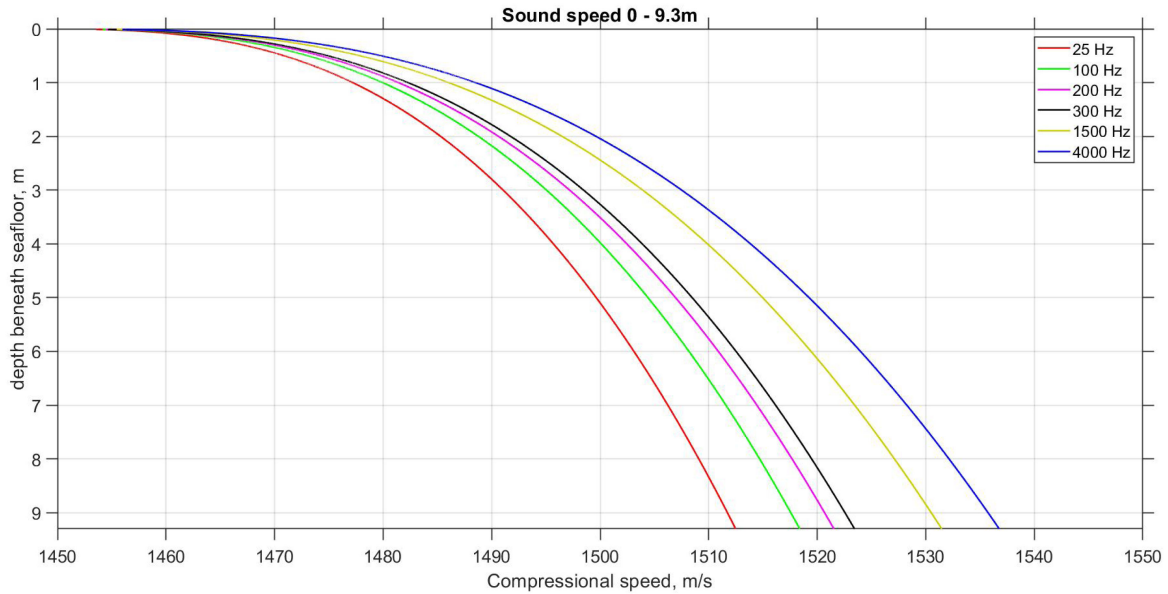
Fig. 7. Predicted depth dependence of mud sediment compressional sound speed versus depth in the 25–4000-Hz band.

speed, there is little frequency dispersion in the 1500–4000-Hz band. However, the sound-speed gradient has a strong nonlinear depth dependence. For example, in the depth interval 0–2 m, the sound speed changes from about 1456 m/s to about 1498 m/s. This gives an average gradient of about 21 (1/s). From 2 to 9.3 m, the sound speed changes from 1498 m/s to about 1535 m/s, for an average gradient of about 5.1 (1/s). The average gradient over the 9.3 m layer of the mud is about 8.5 (1/s).

Fig. 7 shows an extension of the bandwidth to the 25–4000-Hz band for the compressional sound speed versus depth using the VGS model. One observes that the predicted sound-speed gradient decreases as the frequency decreases. In the 25–300-Hz band, the average gradient is about 7.1 1/s. In [12], an effective linear gradient for the mud was found to be about 9.5 1/s from SUS data processed in the 25–275-Hz band. Thus, the VGS model with the inclusion of the overburden pressure terms in the compressional and shear modulus provides a possible effective linear gradient.

Fig. 8 shows the predicted SSR and attenuation dispersion predictions based on the mean of $< P(\theta_k) >$ and standard deviations of the porosity N, the strain hardening index n, and the grain bulk density k_g presented in Table III. For these three parameters, we considered the mean of the cumulative distribution, the mean plus the standard deviation, and the mean minus the standard deviation for a total of 27 VGS parameterizations. Then, using these 27 parameterizations the VGS model was utilized to compute the dispersion of the compressional SSR and the attenuation. SSR is the ratio of the compressional sound speed at the surface of the sediment to the sound speed at the bottom of the water column. The span of these curves provides an estimate of the uncertainty for both the SSR and the attenuation. Direct measurements of the sound speed reported by Yang and Jackson [20] in the 2–10-kHz band and by Ballard [30] in the 25–200-kHz band are included in Fig. 8, along with a

included is a low-frequency estimate inferred from an analysis of SUS explosive charges in the 25–275-Hz band [12]. The black box represents direct sound speed measurements made at five locations that span the area around VLA 1 and VLA 2 [20]. The box attempts to show the range of values reported at the different locations where the sediment acoustics speed measurement system (SAMS) was deployed in Mudpatch. The relevant measurements reported in [20] were approximately between VLA 1 and VLA 2, which are close to PC 16 and PC 18 that were collected by Chaytor [5], respectively. Yang and Jackson [20] measured near PC 16 a ratio of about 0.996 and to the SE at PC 18 measured a value of 0.999 in the 2–10-kHz band. The prediction in Fig. 8 is 0.996 at 4 kHz and, thus, is in agreement with [20]. With the exception of the acoustic core measurement at 25 kHz, the measurements of the SSR reported by Ballard [30] lie within the statistical predictions of the VGS model.

The VGS dispersion curve for the SSR is aligned with the coring estimates above 1.5 kHz but shows greater SSR than previously estimated at the lower frequecies. The SSR reported in [12] in the 25–275-Hz band was 0.9775, which falls below the dispersion curves that were inferred in the 1.5–4.0-kHz band. This low-frequency inference did not use a seabed physics model and instead inverted directly for the SSR and a linear gradient. The attenuation was assumed to be about 0.01 dB/m at 1 kHz with an exponent of unity. It is difficult to understand the difference. Whether the VGS model has difficulties at the low frequencies or setting $\tau = \infty$ is not completely correct for the lower frequencies for a mud sediment is an open question.

Finally, Fig. 8 shows the predicted attenuation dispersion curves for the 27 parameterizations, which shows that the mean attenuation is about 0.045 dB/m at 1 kHz using the ensemble average parameter values.
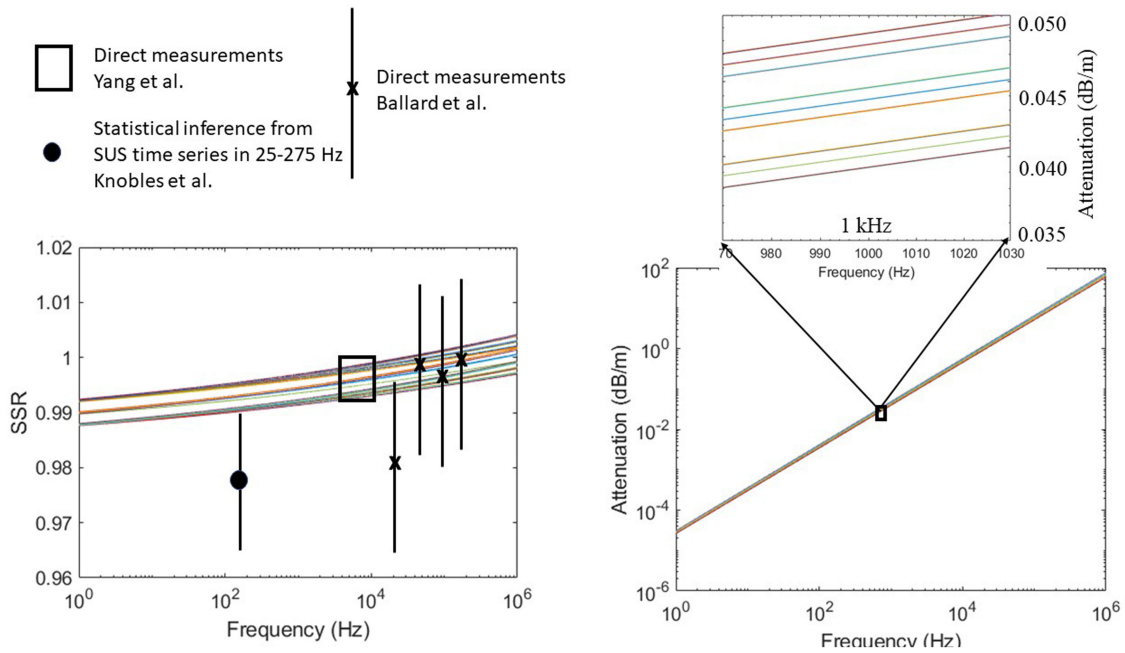
Fig. 8. Predicted SSR and attenuation derived from ITC2015 source data with VGS model compared to direct measurements and the low-frequency estimate in [12]. The 27 smooth curves are those predicted by the VGS model using the average value and standard deviations of N, n, and k_g, which allows for an inference of the uncertainty of the SSR and attenuation.

VI. Conclusion

The predicted dispersion of the SSR in Fig. 8 using two statistical measures and the VGS model are consistent with the direct measurements made by Yang and Jackson with the seabed acoustics measurements system (SAMS). The unique feature of this sediment is that its SSR is generally less than unity with a very weak frequency dependence of the sound speed over a large bandwidth. An important point is that the VGS predictions for the SSR and the attenuation obey a Kramers–Kronig dispersion relationship. The inclusion of this important principle of physics removes nonphysical parameter estimates for sound speed and attenuation that in turn can lead to erroneous sonar predictions.

The analysis suggests that the five data samples analyzed belong to the same statistical distribution, which in turn suggests that the mud variability in the area of the tow track rectangle around the two VLAs is generally small. From the TL data-model comparisons, both the average frequentist and the ensemble-averaged $E(\theta_k)$ solutions generally produce TL predictions that qualitatively match the measured data. The marginal distributions for the porosity N and strain hardening index n are single peaked functions and have only a small degree of skewness. While the distributions for k_g are generally flat in the assumed prior bounds, they do not appear to cause significant uncertainty in N and n. These observations are consistent with the small difference in the predicted sound speed and attenuation dispersion using these two statistical measures.

While the frequentist predictions compare well with those provided by the DEME, one cannot know *a priori* how many data samples are required to produce results that are in agreement.

For the Mudpatch experiment, the measurements were made when the water column was near isospeed. During the warmer months when the water column is stratified and has a larger random component, one can expect the number of data samples required to achieve a similar parameter uncertainty will increase.

Challenges in this work included the fact that the moving source had a 50% duty cycle which, left unaddressed, would allow the inversion model to mistake a time period when the source is off with a modal interference null. To be consistent with the signal processing of the data, the modeled acoustic field underwent the same signal processing before computing the error function on each sampling of the geophysical space. This necessitated the selection of a simple seabed model, a single layer, but with the physics of overburden pressure and sound speed and attenuation frequency dispersion constrained by causality.

A source of uncertainty in this work is that the mud layer may have a thin surface layer, and this layer was not considered in this study. It was found that the five data samples in the 1.5–4.0-kHz band did not appear to support inferring for the geophysical parameters for a two-layer mud model. Thus, the one-layer model should be viewed as an *effective* model for the mud sediment.

The VGS model with the depth dependence modification predicts a large nonlinear sound speed gradient in the mud sediment in the 1.5–4.0-kHz band. Over the larger 25–4000-Hz band while the size of the gradient decreases with decreasing frequency, the frequency dispersion of the sound speed increases with increasing depth into the sediment. Finally, future work is needed to understand the dispersion at the very low frequencies.

REFERENCES

[1] P. S. Wilson, D. P. Knobles, and T. B. Neilsen, "Guest editorial: An overview of seabed characterization experiment," *IEEE J. Ocean. Eng.*, vol. 45, no. 1, pp. 1–13, Jan. 2020.

[2] R. T. Cox, "Probability, frequency, and reasonable expectation," *Amer. J. Phys.*, vol. 14, pp. 1–13, 1946.

[3] D. C. Twichell, C. E. McClennen, and B. Butman, "Morphology and process associated with the accumulation of the fine-grained sediment deposit on the Southern New England Shelf," *J. Sedimentary Petrology*, vol. 51, pp. 269–280, 1981.

[4] J. A. Goff, J. Chaytor, A. Reed, G. Gawarkiewicz, P. S. Wilson, and D. P. Knobles, "Stratigraphic analysis of a sediment pond within the New England Mud Patch: New constraints from high-resolution chirp acoustic reflection data," *Marine Geol.*, vol. 412, pp. 81–94, 2019.

[5] J. Chaytor, M. Ballard, Z. Buczkowski, J. A Goff, K. M. Lee, and A. Reed, "Measurements of geologic characteristics, geophysical properties, and geoacoustic response of sediments from the New England Mud Patch," *IEEE J. Ocean. Eng.*, accepted for publication.

[6] M. J. Buckingham, "Wave propagation, stress relaxation, and grain-to-grain shearing in saturated, unconsolidated marine sediments," *J. Acoust. Soc. Amer.*, vol. 108, pp. 2796–2815, 2000.

[7] M. J. Buckingham, "On pore-fluid viscosity and the wave properties of saturated granular materials including marine sediments," *J. Acoust. Soc. Amer.*, vol. 122, pp. 1486–1501, 2007.

[8] M. J. Buckingham, "Compressional and shear wave properties of marine sediments: Comparisons between theory and data," *J. Acoust. Soc. Amer.*, vol. 117, pp. 137–152, 2005.

[9] M. J. Buckingham, "Wave speed and attenuation profiles in a stratified marine sediment: Geo-acoustic modeling of seabed layering using the viscous grain shearing (VGS) theory," *J. Acoust. Soc. Amer.*, vol. 148, no. 2, pp. 962–974, 2020.

[10] A. Mallock, "The damping of sound by frothy liquids," *Proc. Roy. Soc.*, vol. 84A, no. 572, pp. 391–395, 1910.

[11] A. B. Wood, *A Textbook of Sound*, 1st ed. New York, NY, USA: MacMillan, 1930.

[12] D. P. Knobles *et al.*, "Maximum entropy derived statistics of sound speed structure in a fine-grained sediment inferred from sparse broadband acoustic measurements on the New England Continental Shelf," *IEEE J. Ocean. Eng.*, vol. 45, no. 1, pp. 161–173, Jan. 2020.

[13] M. D. Richardson and K. B. Briggs, "Empirical predictions of seafloor properties based on remotely measured sediment impedance," in *High Frequency Ocean Acoustics*, M. Porter, M. Siderius, and W. A. Kuperman, Eds. College Park, MD, USA: AIP, 2004.

[14] W. C. Krumbein, "Size frequency distributions of sediments," *J. Sedimentary Petrology*, vol. 4, no. 2, pp. 65–77, 1934.

[15] H. A. Kramers, "La diffusion de la lumire par les atomes," *Atti Congresso Internationale Fisici (Trans. Volta Centenary Congr.) Como*, vol. 2, pp. 545–557, 1927.

[16] R. de L. Kronig, "On the theory of the dispersion of X-rays," *J. Opt. Soc. Amer.*, vol. 12, no. 6, pp. 547–557, 1926.

[17] L.D.Landau and E.M. Lifshitz, *Electrodynamics of Continuous Media*. Moscow, Russia: Pergamon, 1981.

[18] J. Belcourt, C. W. Holland, S. E. Dosso, J. Dettmer, and J. A. Goff, "Depth-dependent geoacoustic inferences with dispersion in the New England MudPatch via reaction coefficient inversion," *IEEE J. Ocean. Eng.*, vol. 45, no. 1, pp. 69–91, Jan. 2020.

[19] J. Bonnel, S. E. Dosso, D. Eleftherakis, and N. R. Chapman, "Trans-dimensional inversion of modal dispersion data on the New England Mud Patch," *IEEE J. Ocean. Eng.*, vol. 45, no. 1, pp. 116–130, Jan. 2020.

[20] J. Yang and D. R. Jackson, "Measurement of sound speed in fine-grained sediments during the seabed characterization experiment," *IEEE J. Ocean. Eng.*, vol. 45, no. 1, pp. 39–50, Jan. 2020.

[21] E. K. Westwood, C. T. Tindle, and N. R. Chapman, "A normal mode model for acoustoelastic ocean environments," *J. Acoust. Soc. Amer.*, vol. 100, pp. 3631–3645, 1996.

[22] I. Goodfellow, Y. Bengio, and A. Courville, *Deep Learning*. Cambridge, MA, USA: MIT Press, 2016, ch. 4.

[23] D. P. Knobles, J. D. Sagers, and R. A. Koch, "Maximum entropy approach for statistical inference in an ocean acoustic waveguide," *J. Acoust. Soc. Amer.*, vol. 131, pp. 1087–1101, 2012.

[24] D. P. Knobles, "Maximum entropy inference of seabed attenuation parameters using ship radiated broadband noise," *J. Acoust. Soc. Amer.*, vol. 138, pp. 3563–3575, 2015.

[25] S. Kullback and R. A. Leibler, "On information and sufficiency," *Ann. Math. Statist.*, vol. 22, pp. 79–86, 1951.

[26] E. T. Jaynes, "Information theory and statistical mechanics," *Phys. Rev.*, vol. 106, pp. 620–630, 1957.

[27] E. T. Jaynes, "Information theory and statistical mechanics: II," *Phys. Rev.*, vol. 108, pp. 171–190, 1957.

[28] G. Bilbro and D. E. Van den Bout, "Maximum entropy and learning theory," *Neural Comput.*, vol. 4, pp. 839–853, 1992.

[29] E. T. Jaynes *Probability Theory The Logic of Science.* Cambridge U.K.: Cambridge Univ. Press, 2007.

[30] M. S. Ballard, K. M. Lee, A. R. McNeese, P. S. Wilson, J. D. Chaytor, and J. A. Goff, "In situ measurements of compressional wave speed during gravity coring operations in the New England Mud Patch," *IEEE J. Ocean. Eng.*, vol. 45, no. 1, pp. 26–38, Jan. 2020.

David Paul Knobles received the Ph.D. degree in nuclear theory from the University of Texas at Austin, Austin, TX, USA, in 1989.

From 1989 to 1992, he did a Postdoctoral Fellowship in Nuclear Physics with the University of Texas at Austin. He is currently an owner of Knobles Scientific and Analysis (KSA), a private business that specializes in defense and environmental applications. His research interests include theoretical physics, remote sensing, cosmology, and bioacoustics.

Dr. Knobles is currently a Co-Chief Scientist for the ONR Seabed Characterization Experiment.

Christian D. Escobar-Amado received the Bachelor of Science degree in electronics engineering from the Francisco de Paula Santander University, Cucuta, Colombia, in 2016. He has been working toward the Ph.D. degree in electrical and computer engineering with the University of Delaware, Newark, DE, USA, since 2019.

From 2017 to 2018, he was a Junior Researcher with the Administrative Department of Science, Technology, and Innovation, also known as Colciencias, Bogotá, Colombia. His research interests include shallow water acoustics, Bayesian optimization methods, and physics-based deep learning techniques applied to ocean acoustics.

Dr. Escobar-Amado was awarded an internship with the Ocean Acoustic Engineering Laboratory, University of Delaware and subsequently admitted to the graduate program there.

Michael J. Buckingham received the B.Sc. (Hons.) degree in physics and the Ph.D. degree in solid state physics from the University of Reading, Reading, U.K., in 1967 and 1971, respectively.

He is currently a Distinguished Professor of Ocean Acoustics with the Marine Physical Laboratory, Scripps Institution of Oceanography (Scripps), University of California, San Diego, La Jolla, CA, USA. He has been a Visiting Professor with the Institute of Sound and Vibration Research, University of Southampton, Southampton, U.K., with the National Key Laboratory of Science and Technology on Sonar, Hangzhou, China, and with the Department of Ocean Engineering, Massachusetts Institute of Technology, Cambridge, MA, USA. Before joining Scripps, he was an Individual Merit Senior Principal Scientific Officer with the Royal Aerospace Establishment, Farnborough, U.K. While with RAE, he was an Exchange Scientist, attached to the British Embassy, with the Naval Research Laboratory, Washington, DC, USA. He authored a book *Noise in Electronic Devices and Systems* (Wiley, 1983), and he is a coeditor of *Sea Surface Sound 1994, Proceedings of the III International Meeting on Natural Physical Processes Related to Sea Surface Sound*. His research has been reported in more than 250 papers, articles, and reports in the scientific literature.

Dr. Buckingham was the U.K. National Representative on the Scientific Committee of the Marine Science and Technology (MAST) Programme, Commission of European Communities, Brussels, Belgium. Along with several other awards for his research on underwater acoustics, he was the recipient of the A. B. Wood Medal from the Institute of Acoustics, U.K., and the Pioneers of Underwater Acoustics Medal from the Acoustical Society of America. He is a Fellow of the Acoustical Society of America, the Institute of Acoustics (U.K.), and the Institution of Engineering and Technology (U.K.); and he is a Chartered Engineer (U.K.). Recently, he was honored to serve as the Vice President of the Acoustical Society of America. He is currently an Editor-in-Chief of the *Journal of Computational Acoustics*, and he was the Editor of Reviews in Physical Acoustics for the *Journal of Sound and Vibration*.

William S. Hodgkiss (Life Member, IEEE) received the Ph.D. degree in electrical engineering from Duke University, Durham, NC, USA, in 1975.

His current research interests are in the areas of signal processing, communications, propagation modeling, ambient noise, and environmental inversions, with applications of these to underwater acoustics and electromagnetic wave propagation.

Dr. Hodgkiss is a Fellow of the Acoustical Society of America.

Since 1978, he has been a Member of the Faculty of the Scripps Institution of Oceanography, University of California, San Diego, La Jolla, CA, USA, and a Member of Staff of the Marine Physical Laboratory.

Preston S. Wilson received the B.S. and M.S. degrees in mechanical engineering from The University of Texas at Austin (UT Austin), Austin, TX, USA, in 1990 and 1994, respectively, and the Ph.D. degree in mechanical engineering from Boston University, Boston, MA, USA, in 2001, all in mechanical engineering.

He is currently a Raymond F. Dawson Centennial Fellow in Engineering with the University of Texas at Austin, with joint appointments with the Mechanical Engineering Department and with ARL:UT. He was a Research Engineer with the Applied Research Laboratories (ARL:UT) from 1993 to 1997, Postdoctoral Fellow with Boston University from 2001 to 2003, and has been a faculty member with the UT Austin since 2003. He holds six U.S. patents, and is a Co-Founder of AdBm, Inc., Austin, TX, USA, operating in the underwater noise mitigation arena. His work has been reported in more than 360 peer-reviewed papers, conference proceedings, technical reports and published presentation abstracts. He is currently a Co-Chief Scientist for the ONR Seabed Characterization Experiment. His research areas are broadly focused on physical acoustics, underwater acoustics, engineering acoustics, and bioacoustics, with specific areas of interest in sound propagation in shallow water, in water-saturated sediments, bubbly liquid, and multiphase material.

Dr. Wilson was the recipient of the A.B. Wood Medal from the Institute of Acoustics U.K. He is a Fellow of the Acoustical Society of America (ASA), the Past-Chair of the Committee for Education in Acoustics of the ASA, a current member of the Executive Council of the ASA, and an Associate Editor for the *Journal of the Acoustical Society of America*.

Tracianne B. Neilsen (Member, IEEE) received the Ph.D. degree in physics from The University of Texas at Austin, Austin, TX, USA, in 2000.

She is currently an Associate Professor with the Department of Physics and Astronomy, Brigham Young University, Provo, UT, USA. Her Postdoctoral Research was completed with the Applied Research Laboratories, University of Texas at Austin, investigating iterative optimizations for source localization and seabed parameterization in shallow ocean environments. Since 2007, she has been a part-time Research Scientist; her focus shifted to optimizations for high-frequency seabed parametrization using the Biot model. For more than a decade, she was a part-time Assistant Professor with Brigham Young University and did research on jet noise source characterization. In May 2018, she became a full-time Professor and returned to underwater acoustics research. She has recently been applying deep learning in ocean acoustics.

Jie Yang received the B.S. degree in physics from the Ocean University of China, Qingdao, China, in 1999 and the Ph.D. degree in mechanical engineering from the Georgia Institute of Technology, Atlanta, GA, USA, in 2007.

Since 2007, she was a Postdoctoral Fellow supported by the U.S. Office of Naval Research and currently a Principal Physicist with the Applied Physics Laboratory, University of Washington, Seattle, WA, USA. Her research interests include both active and passive acoustics, with the former focusing on mid-frequency sound propagation and reverberation in littoral oceans and the latter on estimating wind speed and rain rate using ocean ambient sound and their relation to global water cycle and climate change.

Dr. Yang is a member of the Acoustical Society of America.

Mohsen Badiey received the Ph.D. degree in applied marine physics and ocean engineering from the Rosenstiel School of Marine and Atmospheric Science, University of Miami, Coral Gables, FL, USA, in 1988.

From 1988 to 1990, he was a Postdoctoral Fellow with the Port and Harbor Research Institute, Ministry of Transport in Japan. After his Postdoctoral Research, he became a faculty member with the University of Delaware, Newark, DE, USA, where he is currently a Professor of Electrical and Computer Engineering and joint Professor in Physical Ocean Science and Engineering. From 1992 to 1995, he was a Program Director and a Scientific Officer with the Office of Naval Research (ONR) where he was the team leader to formulate long-term naval research in the field of Acoustical Oceanography. His research interests are physics of sound and vibration, shallow water acoustics and oceanography, underwater acoustic communications, acoustic signal processing and machine learning, seabed acoustics, and geophysics.

Dr. Badiey is a Fellow of the Acoustical Society of America.